



# Knoevenagel condensation reactions catalyzed by nitrogen-containing mesoporous carbon materials under mild reaction conditions

Bing Xue<sup>1,2</sup> · Lin-Zhi Wen<sup>1</sup> · Dan Ma<sup>1</sup> · Man-Man Li<sup>1</sup> · Jie Xu<sup>1</sup>

Received: 9 April 2018 / Accepted: 28 August 2018 / Published online: 3 September 2018  
© Springer Nature B.V. 2018

## Abstract

A series of nitrogen-containing ordered mesoporous carbon (NOMC) materials have been prepared by a convenient soft-templating method. The physicochemical properties of the NOMC samples were characterized by N<sub>2</sub> adsorption and desorption, small-angle XRD, FT-IR, XPS, and TEM. As solid base catalysts, NOMCs exhibited remarkable catalytic activities for Knoevenagel condensation reactions under mild reaction conditions, depending on their synthetic calcination temperature. Among them, NOMC-500 showed the highest catalytic activity. For Knoevenagel condensation of benzaldehyde and malononitrile, the conversion of aldehyde was higher than 85% under 50 °C. Moreover, the catalysts had good catalytic applicability for wide substrates. The catalytic activity obtained on NOMC catalyst is compared with other nitrogen-containing carbon-based materials.

---

**Electronic supplementary material** The online version of this article (<https://doi.org/10.1007/s11164-018-3578-7>) contains supplementary material, which is available to authorized users.

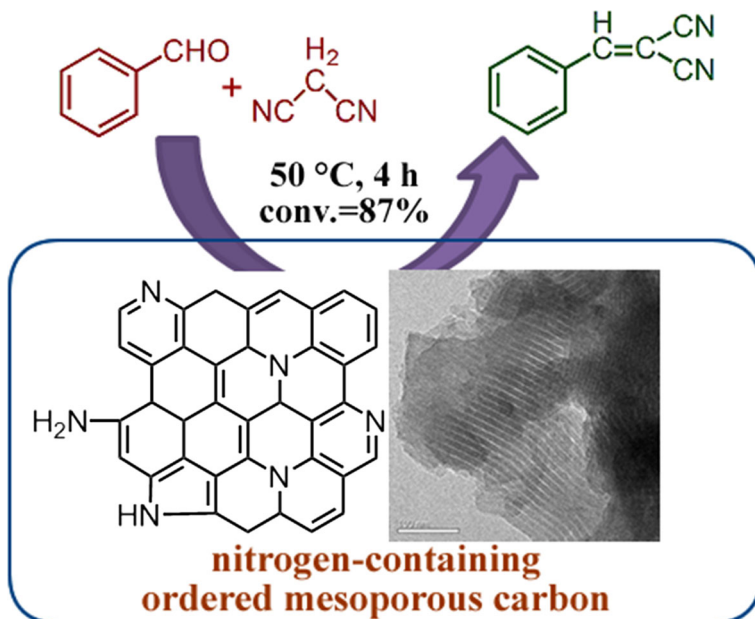
---

✉ Jie Xu  
shine6832@163.com

Extended author information available on the last page of the article

## Graphical abstract

Nitrogen-containing ordered mesoporous carbon materials, prepared by a soft-templating method under aqueous solution and as solid base catalysts, demonstrated high catalytic activity in Knoevenagel condensation reactions under mild reaction conditions.



**Keywords** Base catalysis · Knoevenagel condensation · Nitrogen-containing carbon · Mesoporous carbon

## Introduction

Knoevenagel condensation reactions of aldehydes and active methylene-containing compounds are among the most primary processes in synthetic chemistry for C=C bond formation [1], and are extensively used in the manufacture of therapeutic drugs, polymers, perfume [2], etc. Traditionally, Knoevenagel condensation is performed homogeneously by Lewis bases and acids, such as pyridine, piperidine, alkali metal hydroxides, and transition metal halides [3]. Despite their high catalytic activities, the major disadvantage associated with the use of such catalysts lies in the difficulty in catalyst-product separation along with product purification [3]. Some heterogeneous catalysts represented by alkaline earth oxides, clay, and hydrotalcites could technically solve the separation issue, while simultaneously bringing out salt and potential metal contamination to the final products [4, 5]. On the other hand, amines [6] and ionic liquids [7] immobilized on silica supports, notwithstanding

their good catalyst recyclability, also suffer from high cost of coupling agents and time-consuming grafting procedures.

Recently, several groups, including ours, have reported that carbon nitride materials, as new types of metal-free materials, could catalyze numerous Knoevenagel condensation [4, 8–11] and transesterification reactions [12–14] owing to their rich nitrogen-containing groups. Unfortunately, most of the mesoporous carbon nitride materials are prepared by nanocasting methods adopting siliceous materials as sacrificial hard templates, which require a subsequent silica-etching step using HF solution [15–17]. In addition to carbon nitride, nitrogen-doped carbon materials have been recently applied as solid base catalysts for Knoevenagel condensation. These nitrogen-doped carbon materials include, for instance, *N*-doped graphene [18], amine-containing active carbon [19], PAN-C500-AO400 prepared using polyacrylonitrile via ammoxidation [20], etc. However, such materials demanded high reaction temperatures ( $> 70$  °C), and the catalytic yields of the target molecule were not satisfactory. Therefore, it is highly desirable to explore and develop a new metal-free heterogeneous catalyst for Knoevenagel condensation reactions.

Like carbon nitride and graphene oxide, nitrogen-containing ordered mesoporous carbon (NOMC) is a new type of metal-free material. Owing to its large surface area, accessible and ordered mesopores, and inherent incorporation of nitrogen atoms into the carbon framework, NOMC materials have recently demonstrated wide application in CO<sub>2</sub> capture [21], supercapacitors [22], and heterogeneous catalysis [23–25]. In particular, NOMC possesses various types of nitrogen-containing groups in forms of pyridine, pyrrole, etc, which enable it as a typical solid base [26]. Nevertheless, to the best of our knowledge, except for transesterification reactions of  $\beta$ -keto esters [26], the application of NOMC materials as solid catalysts in other base-mediated organocatalysis is quite limited. In this contribution, we synthesized NOMC materials and then employed them as solid catalysts in Knoevenagel condensation reactions of a variety of aldehydes and malononitrile. NOMC materials demonstrated catalytic activities that depended on the calcination temperature of NOMC. Under optimized conditions, the conversion of benzaldehyde reached up to 87% at a reaction time of 4 h under 50 °C. Compared with previously reported nitrogen-containing based materials, the NOMC catalysts were applied under milder temperatures, yet offered catalytic activity that was superior to most of the previously reported mesoporous nitrogen-containing carbon materials.

## Experimental

### Synthesis of NOMC materials

4 g of F127 (EO<sub>106</sub>PO<sub>70</sub>EO<sub>106</sub>) and 0.96 g of 1,3,5-trimethylbenzene were dissolved into 100 mL of H<sub>2</sub>O, and then stirred vigorously for 4 h, followed by addition of 2.2 g of *m*-aminophenol, 1.4 g of hexamethylenetetramine, and 2.6 mL of aqueous ammonia (28 wt%). After 1 h of further stirring, the mixture was heated at 80 °C under vigorous stirring for 24 h. The mixture was subsequently filtered,

and the obtained solid was rinsed by water and ethanol, and dried at 60 °C. After that, the solid was ground, then calcinated under nitrogen atmosphere from room temperature to a desired temperature with a ramping rate of 1 °C min<sup>-1</sup>, and then held at this temperature for 2 h. The final powder was labeled as NOMC-*T*, where *T* represents the calcination temperature.

### Sample characterization

X-ray diffraction (XRD) patterns were recorded with a Rigaku D/max 2500 PC X-ray diffractometer equipped with a graphite monochromator (40 kV, 40 mA) using Ni-filtered Cu-*K*α radiation. Nitrogen adsorption–desorption analysis was measured at –196 °C using an ASAP 2020 (Micromeritics) porosimeter. Before the measurement, the samples were degassed at 150 °C for 4 h. The specific surface areas were calculated using the Brunauer–Emmet–Teller (BET) method, and the pore size distributions were determined by Barret–Joyner–Halenda (BJH) model from desorption branches. Transmission electron microscopy (TEM) experiments were carried out on a JEOL 2010 electron microscope. Fourier transform infrared (FT-IR) spectra in transmission mode were recorded on a Tensor 27 (Bruker) spectrometer with the aid of KBr pellets. Each spectrum was measured with a resolution of 4 cm<sup>-1</sup>, using 32 scans at room temperature. X-ray photoelectron spectroscopy (XPS) measurements were carried out on a PHI 5000C (Perkin–Elmer) spectrometer recording with a constant energy mode (Mg *K*α radiation as the excitation source). The subsequent data analysis for XPS was performed by means of the XPS Peak 4.1 program. The backgrounds of the N 1 s and O 1 s spectra were subtracted based on a Shirley function from the region of interest. Afterwards, the spectra were fitted according to the binding energies of various bonding-state atoms (components) described in the relevant literature, wherein the ratio of Lorentzian–Gaussian function for each fitted peak was kept as 20% Lorentzian and 80% Gaussian. The full-width-half-maximum (FWHM) values for the deconvoluted N 1 s and O 1 s spectra were 1.5–1.8 eV and 1.7–1.9 eV, respectively.

### Catalytic evaluation

Knoevenagel condensation was carried out in a flask (25 mL). 5 mmol of malononitrile, 5 mmol of benzaldehyde, 0.5 mL of *n*-decane as an internal standard, and CH<sub>3</sub>CN as a solvent were mixed well, followed by addition of 50 mg of NOMC. The catalytic tests were carried out at 50 °C, and samples of reaction mixture were periodically collected and then analyzed by GC equipped with a SE-54 capillary column.

## Results and discussion

### Catalyst characterization

The surface areas and porous properties of NOMC materials were characterized by the  $N_2$  adsorption–desorption technique. Each sample presents an IV-type isothermal curve (Fig. 1a), along with a hysteric loop appearing at  $p/p_0 = 0.4–0.7$ , suggesting that the NOMC materials contain mesopores. For NOMC-450, it is found that the isotherm curves in the low range of relative pressures ( $p/p_0 < 0.4$ ) are not reversible. This might be due to partial decomposition of the sample under the low pressure of the analytic conditions. On the other hand, as the calcination temperature of NOMC is raised, the NOMC samples reveal larger adsorption quantities in the higher pressure conditions ( $p/p_0 = 0.9–1.0$ ). This implies that higher calcination temperatures would lead to the formation of macropores [23, 27], which might be derived from the voids between particles. Despite this, the average sizes of mesopores of the four materials are still ca. 3.7 nm with relatively concentrated pore size distributions (Fig. 1b). The dependence on calcination temperature is also reflected in surface area and total pore volume. As shown in Table 1, from NOMC-450 to NOMC-550, the surface area increases whereas the pore volume decreases monotonically. However, NOMC-600 has the lowest surface area and pore volume, as the excessively high calcination temperature possibly leads to partial collapse of mesostructures.

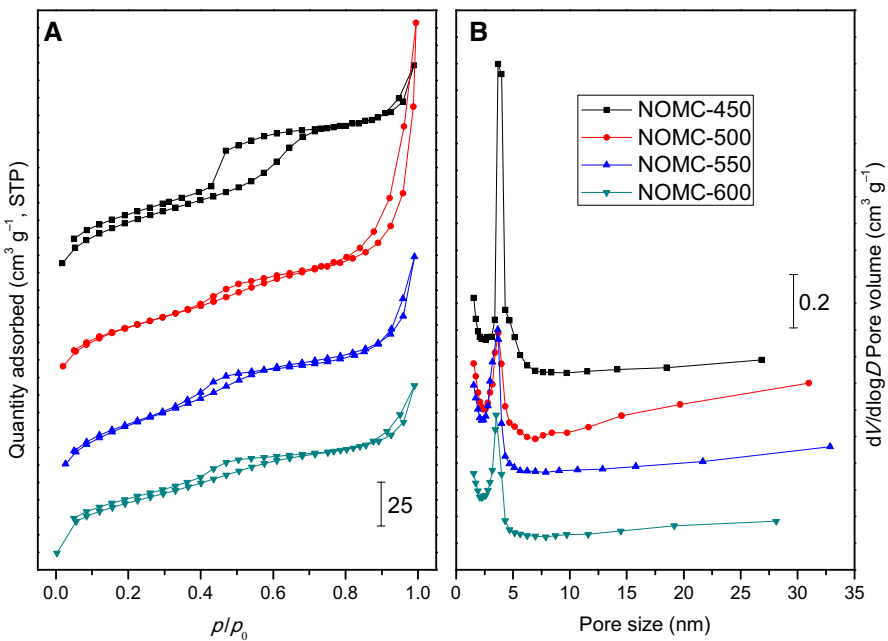


**Fig. 1**  $N_2$  adsorption–desorption isotherms and pore size distributions of NOMC-450, NOMC-500, NOMC-550, and NOMC-600 materials

**Table 1** Textural parameters and chemical compositions of NOMC materials

Sample	$S_{\text{BET}}$ ( $\text{m}^2 \text{g}^{-1}$ )	Pore size <sup>a</sup> (nm)	Pore volume ( $\text{cm}^3 \text{g}^{-1}$ )	Percentage of element <sup>b</sup>		
				C	N	O
NOMC-450	344	3.67	0.30	85.1	8.4	6.5
NOMC-500	395	3.70	0.45	84.3	9.2	6.5
NOMC-550	450	3.64	0.36	85.0	8.3	6.7
NOMC-600	370	3.52	0.28	85.6	8.0	6.4

<sup>a</sup>Determined by the adsorption branches

<sup>b</sup>Measured by XPS survey

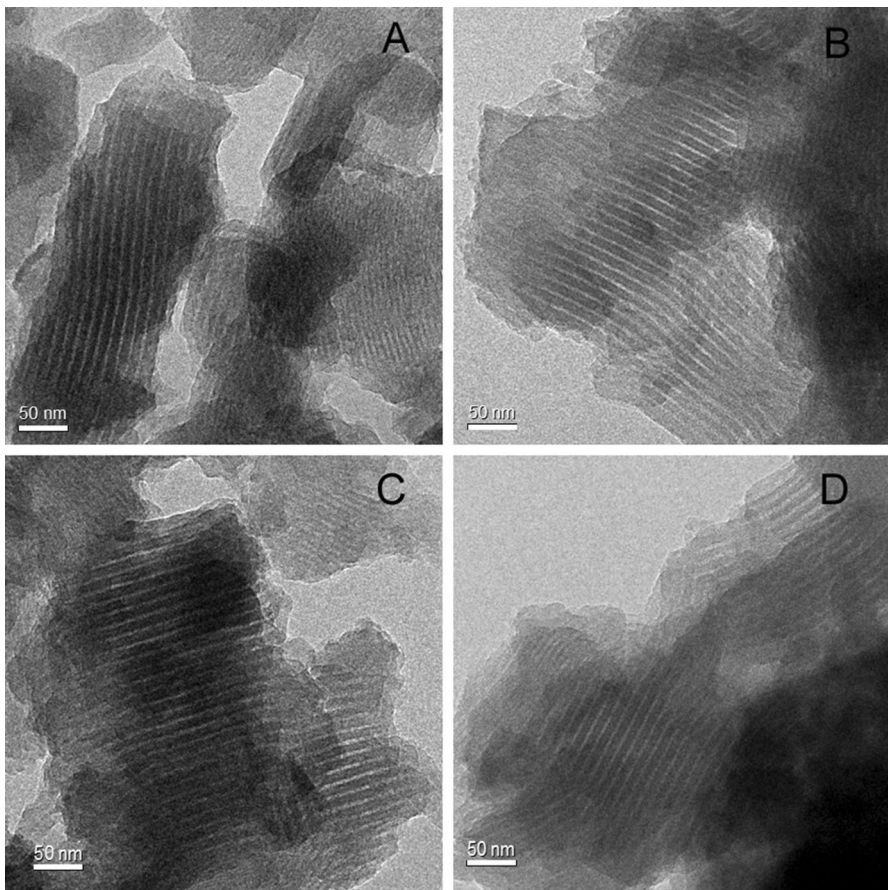


**Fig. 2** TEM images of NOMC-450 (a), NOMC-500 (b), NOMC-550 (c), and NOMC-600 (d) materials

The micro-morphology of the four NOMC materials was analyzed by TEM. The TEM images (Fig. 2) clearly display an ordered planar arrangement, wherein the dark contrast strips represent the carbon walls of NOMC. The pore size may be

directly measured by the width of bright arrays to be ca. 4 nm, in good agreement with the abovementioned  $N_2$  adsorption–desorption results. The order of mesoporous structures of NOMC is further supported by small-angle XRD characterization. As shown in Fig. 3, the XRD patterns of all four samples exhibit a diffraction peak in the range of  $2\theta = 1.15^\circ$ – $1.3^\circ$ , indexed as the (110) planes of two-dimensional hexagonal symmetry [23, 24]. An obvious shift of the diffraction peaks towards large  $2\theta$  values can be detected from NOMC-450 to NOMC-600. This probably originated from the shrinkage of mesoporous channels of NOMC materials under high calcination temperatures [26], which also has been found in other mesoporous carbon materials [21, 23] fabricated through a soft-templating route.

FT-IR spectra of various NOMC materials are depicted in Fig. S1. Each spectrum shows a broad band in the range of 3600 to 3100 (centered at  $3410\text{ cm}^{-1}$ ), which corresponds to N–H symmetric stretching vibration ( $\nu_s$ ) derived from amino functionalities ( $-\text{NH}_2$  and  $-\text{NH}-$ ), also combined with the O–H vibration mode derived from adsorbed water molecules [28–30] on the surface of NOMCs. Another weak but apparent transmittance signal can be detected in  $3020\text{ cm}^{-1}$  in the FT-IR spectrum for each NOMC material; the band is indexed as the C–H stretching vibration of  $-\text{CH}_2-\text{NH}-\text{CH}_2-$  or  $-\text{CH}_2-\text{NH}-\text{CH}_3$  [31]. The sharp band at  $1584\text{ cm}^{-1}$  is indexed as in-plane deformation vibration ( $\beta$ ) of N–H groups [21, 31, 32], and the weak band centered at  $1720\text{ cm}^{-1}$  is associated with C=O groups [33]. The broad peak around  $1250\text{ cm}^{-1}$  is assigned to the C–N stretching vibration and/or C–O–C groups [33]. In addition, the multiple bands emerging in the range of  $950$  to  $650\text{ cm}^{-1}$  correspond to the out-of-plane N–H deformation vibration ( $\omega$ ) [29]. Such characteristic bands pertaining to nitrogen-containing groups verify the existence of basic sites in the NOMC materials, which thereby could be naturally applied as solid base catalysts.

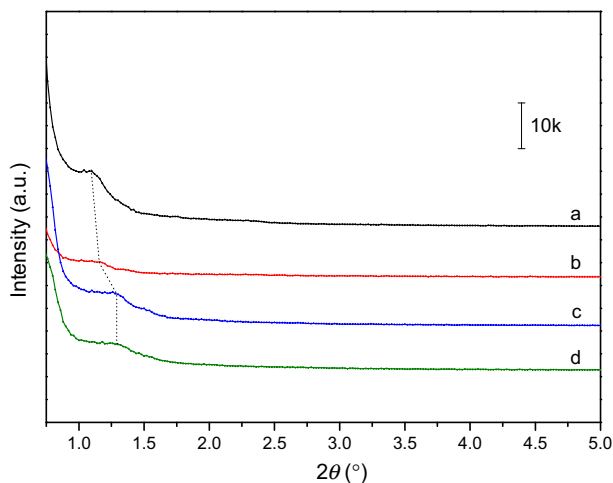


**Fig. 3** Small-angle XRD patterns NOMC-450 (a), NOMC-500 (b), NOMC-550 (c), and NOMC-600 (d) materials

The XPS characterization profile (Fig. S2) verifies the existence of nitrogen elements on the surface of NOMC-500. According to the XPS survey, the concentration of elemental nitrogen on the surface of NOMC materials is discovered to be related to their preparation condition (Table 1). As the table shows, NOMC-500 has superior nitrogen concentration (9.2%) to other three NOMC materials; however, the difference with regard the percentage of total nitrogen is relatively slight. For the purpose of further analysis of the bonding states of nitrogen species, deconvolution of N 1s spectra of NOMC-500 (Fig. 4) and NOMC-450 (Fig. S3) as examples was conducted. Each spectrum is divided into four peaks. The primary peak with the lowest binding energy of 398.4 eV corresponds to pyridinic-type nitrogen atoms, which account for a major portion of the total nitrogen species [21]. The peak centered at 400.1 eV is ascribed to pyrrolic nitrogen atoms, while the signal at 400.9 eV is associated with graphitic atoms and/or amino groups located at the edge of graphitic sheets of NOMC [21, 23]. The last peak with the lowest intensity is derived from quaternary nitrogen species and/or oxidized nitrogen.

Table 2 lists the detailed distributions of various nitrogen species of NOMC materials. As the temperature is elevated, the percentage of pyridinic nitrogen shows a distinct decline, whereas the percentage of pyrrolic nitrogen exhibits a noticeable increase. In the case of other nitrogen species, including quaternary nitrogen species and/or oxidized nitrogen, the proportion shows no apparent variation. It is noted that with regard to the distribution of graphitic nitrogen, NOMC-500 possesses the highest values. More specifically, the order of the percentage of graphitic nitrogen in NOMC materials is NOMC-500 > NOMC-550 > NOMC-600 > NOMC-450. This finding agrees well with some published papers [10, 30, 31], in which it was reported that the calcination or carbonization temperatures could substantially influence the distributions of nitrogen species.

The detailed O 1s spectrum of NOMC-500 is depicted in Fig. 5, and the whole peak could be divided into three major signals. The peak with the lowest binding

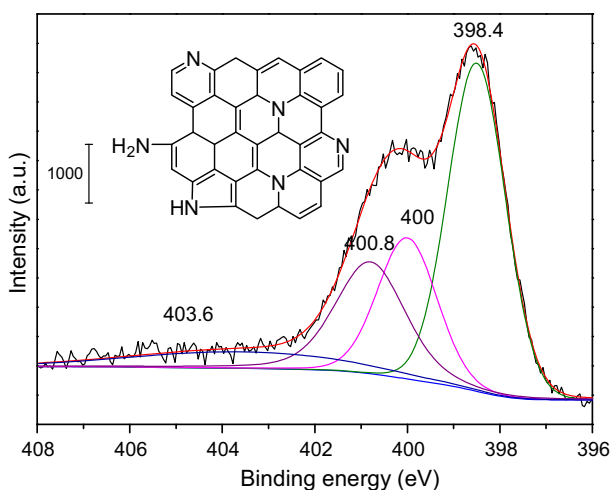


**Fig. 4** N 1s spectrum of NOMC-500 sample



**Table 2** Distributions of various nitrogen species of NOMC materials

Material	Pyridinic N (%)	Pyrrolic N (%)	Graphitic N (%)	Others (%) <sup>a</sup>
NOMC-450	53.1	20.9	16.8	9.2
NOMC-500	47.4	21.6	22.0	9.0
NOMC-550	47.1	23.0	20.6	9.3
NOMC-600	44.5	26.3	18.8	10.3

Determined by XPS

<sup>a</sup>Quaternary nitrogen species and/or oxidized nitrogen

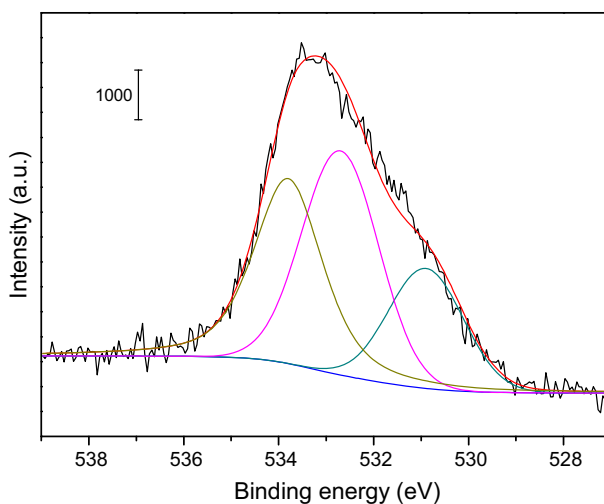


**Fig. 5** O 1s spectrum of NOMC-500 sample

energy (530.9 eV) is assigned to carbon atoms in quinone units [23]. The peaks centered at 532.7 and 533.8 eV correspond to carbon atoms bonded in forms of C=O and C–OH groups. These various carbon species agree with the above FT-IR analysis.

### Catalyst performance

Firstly, a blank test without any catalyst was performed and only 5% of benzaldehyde was converted (Table 3). Using NOMC-450 as a catalyst, the conversion is 36% and the selectivity to the target molecule (2-benzylidene-malononitrile) is above 99%. That is, almost no byproduct was obtained under the reaction conditions. It is evident that the catalytic activities depend on the calcination temperature, and NOMC-500 demonstrates the highest conversion (87%). In the cases of NOMC samples with higher calcination temperatures in synthetic procedures, the catalytic activity decreases drastically. As explained above, XPS characterization results reveal that there exist four types of nitrogen

**Table 3** Catalytic performances of various NOMC materials in Knoevenagel condensation reactions

Catalyst	Conv. (%)	Sel. (%)
–	5	> 99
NOMC-450	36	> 99
NOMC-500	87	> 99
NOMC-550	68	> 99
NOMC-600	45	> 99
OMC-500	28	> 99

Reaction conditions: 5 mmol of benzaldehyde, 5 mmol of malononitrile,  $W_{\text{catal.}} = 50$  mg,  $T = 50$  °C, and  $t = 4$  h. The conversions calculated based on benzaldehyde

species on the surface of NOMC, and NOMC-500 owns the highest proportion of graphitic nitrogen species. Referring to the catalytic performances of NOMCs in Knoevenagel condensation, it can be confirmed that the order of catalytic activity correlates well with the percentage of graphitic nitrogen species. This suggests that the graphitic nitrogen species are probably the active sites of NOMCs in Knoevenagel condensation. The finding, in fact, agrees well with the work reported by Zhang et al [30], where the graphitic nitrogen species of mesoporous carbon nitride materials were regarded as the catalytically active sites in Knoevenagel condensation.

Since the O 1 s spectrum of NOMC-500 has revealed that the material has various oxygen-containing species (Fig. 5), which might be considered as catalytically active species for Knoevenagel condensation. Regarding this point, we also prepared an ordered mesoporous carbon (OMC-500) material using resorcinol instead of *m*-aminophenol as a precursor. It is worth noting that the preparation procedure of OMC-500 was identical to that applied in NOMC-500. As listed in Table 3, the catalytic activity obtained over OMC-500 is comparatively lower (28%) than that of NOMC-500 (87%). The comparison indicates that the oxygen-containing species can contribute to the catalytic reaction. However, the primary catalytic active sites of NOMC materials in Knoevenagel condensation are still basic nitrogen-containing species rather than oxygen-containing species. In fact, some papers [10, 30] involving the synthesis of nitrogen-containing mesoporous carbon materials have also reported similar results, that the nitrogen-containing species acted as active solid bases in Knoevenagel condensation reactions.

The influences of reaction temperature and catalyst feeding weight on the catalytic performances are further investigated using NOMC-500 as a reference catalyst. Under a low reaction time of 30 min, the conversion of benzaldehyde is up to 40% (Fig. 6a). Further elevating reaction temperature leads to a smooth increment of the catalytic conversion, whereas adopting higher temperature shows no remarkable increase of conversion. Furthermore, catalyst weight has an evident effect on the final catalytic results (Fig. 6b). As the weight is increased from 10 to 40 mg, the conversion increases progressively. Likewise, the conversion value seems to level off upon adding further catalyst. Fig. S4 plots the catalytic conversion

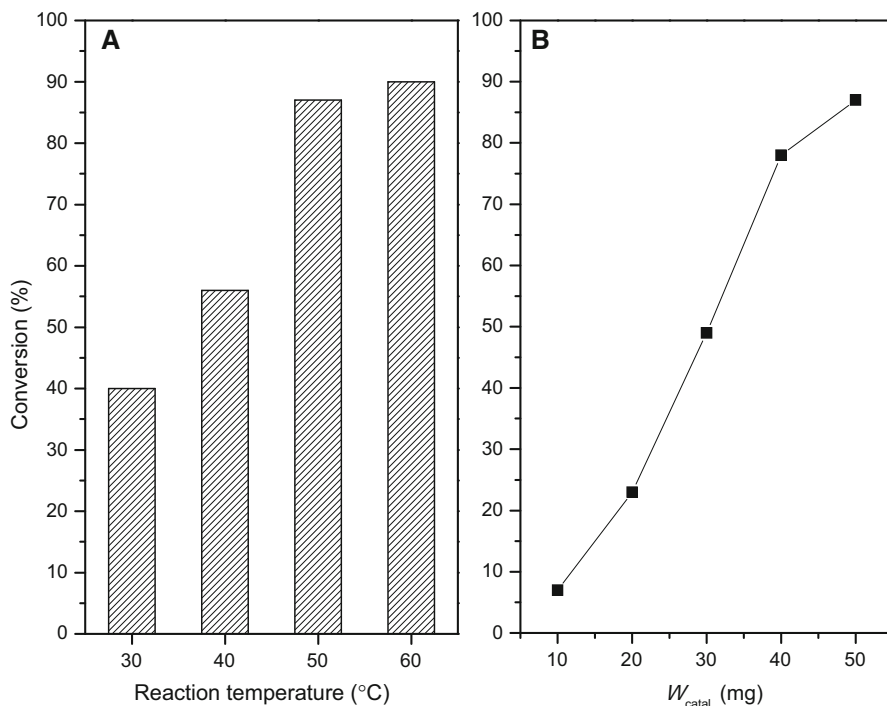


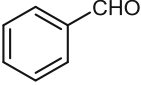
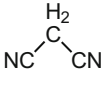
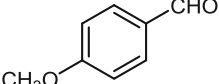
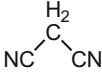
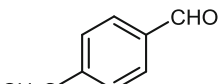
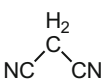
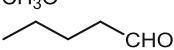
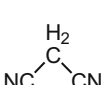
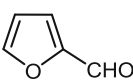
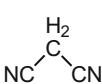
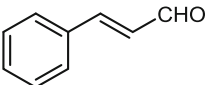
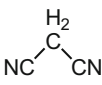
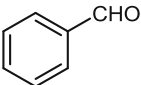
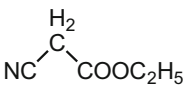
**Fig. 6** Effect of reaction temperature (a) and catalyst weight (b) on the catalytic results over NOMC-500. Reaction conditions: 5 mmol of benzaldehyde, 5 mmol of malononitrile,  $t = 4$  h, catalyst 50 mg (a), and 50 °C (b). The catalytic selectivity for each case is more than 99%

as a function of reaction time. It is found that at the initial 1 h, 45% of benzaldehyde could be catalytically converted. The Knoevenagel reaction reaches its equilibrium after 4 h, affording a maximum catalytic conversion of ca. 90%.

To examine the catalytic versatility of the NOMC catalyst, several Knoevenagel reactions of various aldehyde and methylene-containing compounds were performed. As listed in Table 4, besides benzaldehyde, other aldehydes (including 4-methoxybenzaldehyde, pentanal, furfural, and cinnamaldehyde) apparently could be converted under the same reaction conditions. However, in order to achieve good catalytic productivity, other aldehydes demand longer reaction time, which should be due to their lower activity than benzaldehyde. Moreover, the NOMC catalyst is also able to promote Knoevenagel condensation between benzaldehyde and ethyl cyanoacetate.

Besides the substrate scope, we also evaluated the recyclability of the NOMC catalyst. After each catalytic run, the NOMC-500 sample was filtered, rinsed by ethanol, and reused for the subsequent catalytic test. As illustrated in Fig. 7, during five consecutive runs, the catalytic conversion of benzaldehyde shows no obvious decline, suggesting the NOMC catalysts can be utilized as stable heterogeneous catalysts for Knoevenagel condensation.

**Table 4** Various Knoevenagel condensation reactions catalyzed by NOMC-500

Entry	Aldehyde	Nitrile	Conv. (%)	Sel. (%)
1			87	> 99
2			72	> 99
3 <sup>a</sup>			90	> 99
4			70	> 99
5			76	> 99
6			58	> 99
7			64	> 99

Reaction conditions: 5 mmol of aldehyde, 5 mmol of malononitrile,  $W_{\text{catal.}} = 50$  mg,  $T = 50$  °C, and  $t = 4$  h

<sup>a</sup> $t = 6$  h

For comparison, we summarize the catalytic performances along with reaction conditions of several nitrogen-containing carbon materials in Knoevenagel condensation (Table 5), which have been reported recently. Except that of entry 2, the catalytic reactions of all the entries are higher than room temperature. In general, all the nitrogen-containing carbon materials could promote Knoevenagel condensation reactions with good activity. The highest conversion of benzaldehyde is achieved in MCN-6 and MCN-1 materials; however, the two materials, as well as entries 3–5, were mesoporous materials prepared using silica as hard template. Although the catalytic activity provided in this work is moderate, the NOMC materials have a remarkable advantage in catalyst preparation, as the materials are synthesized by a facile soft-templating method.

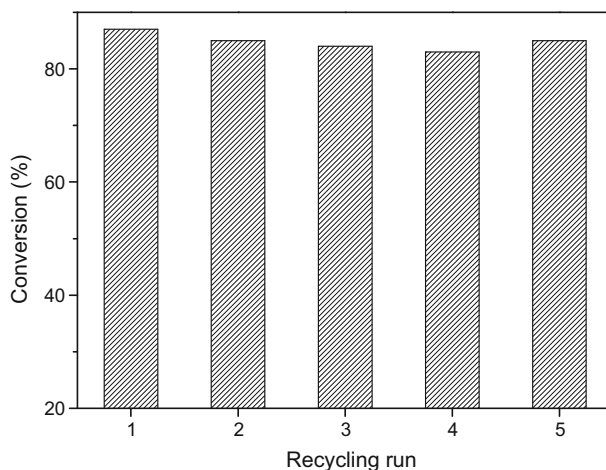


**Fig. 7** Evolution of Knoevenagel reactions during five catalytic runs over NOMC-500. Reaction conditions: 5 mmol of benzaldehyde, 5 mmol of malononitrile,  $W_{\text{catal.}} = 50$  mg,  $T = 50$  °C, and  $t = 4$  h. The selectivity was more than 99% during the catalytic test

**Table 5** Comparison of catalytic performances of various nitrogen-based carbon materials in Knoevenagel condensation of benzaldehyde

Entry	Catalyst	$n_{\text{BAH}}$ (mmol)	$T$ (°C)	$W_{\text{catal.}}$ (mg)	$t$ (h)	Conv. (%)	Sel. (%)	Ref
1	MCN-1 <sup>a</sup>	1	40	20	2	99	100	[30]
2	MCN-6-130 <sup>a</sup>	–	25	20	4	90	> 99	[8]
3	CN-MCF <sup>a</sup>	5	90	100	4	84	94	[10]
4	CND-NaOH <sup>a</sup>	20	70	100	4	80	93	[9]
5	mesoCN-1.5 <sup>a</sup>	5	90	75	5	81	96	[34]
6	<i>N</i> -doped carbon <sup>b</sup>	10	80	100	1	50	> 99	[35]
7	mp-PBI <sup>c</sup>	1	100	100	6	> 99	> 99	[36]
8	PAGO <sup>d</sup>	6	70	20	4	53	> 99	[37]
9	NOMC-500	5	50	50	4	87	> 99	This work

<sup>a</sup>Prepared using mesoporous silica as sacrificial hard template. <sup>b</sup>Prepared by ammoxidation of activated carbon. <sup>c</sup>Mesoporous poly(benzimidazole) material. <sup>d</sup>Graphene oxide modified by propylamine

## Conclusion

NOMC materials have been synthesized by adopting various calcination temperatures, and possess ordered mesopores and large surface areas ( $344\text{--}450$  m<sup>2</sup> g<sup>−1</sup>). The calcination temperature could not only affect the percentage of total elemental nitrogen of NOMC, but also has a significant impact on the distribution of various

nitrogen species. The NOMC materials contain various nitrogen species including pyridinic, pyrrolic, graphitic nitrogen atoms, etc. on the surface. Among the four NOMC materials, The NOMC-500 sample exhibits the highest catalytic activity in Knoevenagel condensation reactions of benzaldehyde and malononitrile. The superior catalytic activity of NOMC-500 is attributed to its highest percentage of graphitic nitrogen atoms, which are probably responsible for the catalytically active sites. Owing to the convenient and eco-friendly synthetic method, together with good recyclability and activity, the NOMC materials could be utilized as catalytic candidates for wider base-mediated organocatalysis.

**Acknowledgements** The work was supported by PetroChina Innovation Foundation (2018D-5007-0508), Advanced Catalysis and Green Manufacturing Collaborative Innovation Center (ACGM2016-06-28), Foundation of State Key Laboratory of High-efficiency Utilization of Coal and Green Chemical Engineering (2017-K28), the Top-notch Academic Programs Project of Jiangsu Higher Education Institutions (PPZY2015B145), and the Priority Academic Program Development of Jiangsu Higher Education Institutions.

## References

1. X. Zhang, E.S. Man Lai, R. Martin-Aranda, K.L. Yeung, *Appl. Catal. A* **261**, 109 (2004)
2. F. Ouyang, Y. Zhou, Z. Li, N. Hu, D. Tao, *Korean J. Chem. Eng.* **31**, 1377 (2014)
3. S. Saravanamurugan, M. Palanichamy, M. Hartmann, V. Murugesan, *Appl. Catal. A* **298**, 8 (2006)
4. M.B. Ansari, H. Jin, M.N. Parvin, S.-E. Park, *Catal. Today* **185**, 211 (2012)
5. S. van Dommele, K.P. de Jong, J.H. Bitter, *Topic. Catal.* **52**, 1575 (2009)
6. S.-E. Park, D.-S. Han, S.-C. Han, M.-J. Jin, T. Ohsuna, *Chem. Commun.* **39**, 4131–4133 (2006)
7. M.N. Parvin, H. Jin, M.B. Ansari, S.-M. Oh, S.-E. Park, *Appl. Catal. A* **413–414**, 205 (2012)
8. S.N. Talapaneni, S. Anandan, G.P. Mane, C. Anand, D.S. Dhawale, S. Varghese, A. Mano, T. Mori, A. Vinu, *J. Mater. Chem.* **22**, 9831 (2012)
9. J. Xu, Y. Wang, J.-K. Shang, Q. Jiang, Y.-X. Li, *Catal. Sci. Technol.* **6**, 4192 (2016)
10. J. Xu, K. Shen, B. Xue, Y.-X. Li, Y. Cao, *Catal. Lett.* **143**, 600 (2013)
11. N.D. Shcherban, P. Mäki-Arvela, A. Aho, S.A. Sergiienko, P.S. Yaremov, K. Eränen, D.Y. Murzin, *Catal. Sci. Technol.* **8**, 2928 (2018)
12. X. Jin, V.V. Balasubramanian, S.T. Selvan, D.P. Sawant, M.A. Chari, G.Q. Lu, A. Vinu, *Angew. Chem. Int. Ed.* **48**, 7884 (2009)
13. J. Xu, K.-Z. Long, T. Chen, B. Xue, Y.-X. Li, Y. Cao, *Catal. Sci. Technol.* **3**, 3192 (2013)
14. C. Anand, S.V. Priya, G. Lawrence, G.P. Mane, D.S. Dhawale, K.S. Prasad, V.V. Balasubramanian, M.A. Wahab, A. Vinu, *Catal. Today* **204**, 164 (2013)
15. J. Zhu, P. Xiao, H. Li, S.A.C. Carabineiro, A.C.S. *Appl. Mater. Inter.* **6**, 16449 (2014)
16. Y. Wang, Q. Jiang, J.-K. Shang, J. Xu, Y.-X. Li, *Acta Phys. -Chim. Sin.* **32**, 1913 (2016)
17. J. Xu, K.-Z. Long, Y. Wang, B. Xue, Y.-X. Li, *Appl. Catal. A* **496**, 1 (2015)
18. T. Tanabe, Y. Yamada, J. Kim, M. Koinuma, S. Kubo, N. Shimano, S. Sato, *Carbon* **109**, 208 (2016)
19. D.P. Bezerra, D.C.S. Azevedo, L.G. Pinheiro, J.M. Filho, A.C. Oliveira, *Chem. Eng. J.* **264**, 565 (2015)
20. S. Fujita, A. Katagiri, H. Watanabe, S. Asano, H. Yoshida, M. Arai, *ChemCatChem* **7**, 2965 (2015)
21. J. Yu, M. Guo, F. Muhammad, A. Wang, F. Zhang, Q. Li, G. Zhu, *Carbon* **69**, 502 (2014)
22. J. Wei, D. Zhou, Z. Sun, Y. Deng, Y. Xia, D. Zhao, *Adv. Funct. Mater.* **23**, 2322 (2013)
23. J. Wang, H. Liu, J. Diao, X. Gu, H. Wang, J. Rong, B. Zong, D.S. Su, *J. Mater. Chem. A* **3**, 2305 (2015)
24. J. Wang, H. Liu, X. Gu, H. Wang, D.S. Su, *Chem. Commun.* **50**, 9182 (2014)
25. D. Ma, H. Zheng, H.-M. Wan, Y. Chen, J. Xu, B. Xue, *Micropor. Mesopor. Mater.* **258**, 244 (2018)
26. J. Xu, D. Ma, Y. Chen, Y. Wang, Y.-X. Li, *Micropor. Mesopor. Mater.* **241**, 72 (2017)
27. N.D. Shcherban, P.S. Yaremov, V.G. Ilyin, M.V. Ovcharova, *J. Anal. Appl. Pyrol.* **107**, 155 (2014)
28. N. Liu, L. Yin, C. Wang, L. Zhang, N. Lun, D. Xiang, Y. Qi, R. Gao, *Carbon* **48**, 3579 (2010)

29. Q. Li, J. Yang, D. Feng, Z. Wu, Q. Wu, S.S. Park, C.-S. Ha, D. Zhao, *Nano Res.* **3**, 632 (2010)
30. L. Zhang, H. Wang, Z. Qin, J. Wang, W. Fan, *RSC Adv.* **5**, 22838 (2015)
31. G.-P. Hao, W.-C. Li, D. Qian, A.-H. Lu, *Adv. Mater.* **22**, 853 (2010)
32. J. Jiang, Q. Gao, Z. Zheng, K. Xia, J. Hu, *Int. J. Hydrogen Energy* **35**, 210 (2010)
33. D.-H. Lan, F.-M. Yang, S.-L. Luo, C.-T. Au, S.-F. Yin, *Carbon* **73**, 351 (2014)
34. J. Xu, Y. Wang, J.-K. Shang, D. Ma, Y.-X. Li, *Appl. Catal. A* **538**, 221 (2017)
35. N. Kan-Nari, S. Okamura, S.-I. Fujita, J.-I. Ozaki, M. Arai, *Adv. Synth. Catal.* **352**, 1476 (2010)
36. P. Makowski, J. Weber, A. Thomas, F. Goettmann, *Catal. Commun.* **10**, 243 (2008)
37. Y. Zhang, C. Chen, G. Wu, N. Guan, L. Li, J. Zhang, *Chem. Commun.* **50**, 4305 (2014)

## Affiliations

Bing Xue<sup>1,2</sup> · Lin-Zhi Wen<sup>1</sup> · Dan Ma<sup>1</sup> · Man-Man Li<sup>1</sup> · Jie Xu<sup>1</sup>

- <sup>1</sup> Jiangsu Key Laboratory of Advanced Catalytic Materials and Technology, School of Petrochemical Engineering, Changzhou University, Gehu Middle Road 21, Changzhou, Jiangsu 213164, People's Republic of China
- <sup>2</sup> State Key Laboratory of Chemical Resource Engineering, Beijing University of Chemical Technology, Beijing 100029, People's Republic of China